Naval Surface Warfare Center
Carderock Division
West Bethesda, MD 20817-5700

NSWCCD-50-TR-2010/024 March 2010

Hydromechanics Department Report

Numerical Simulation of Propeller Performance with an Inclined Shaft Arrangement

by

Seth Schroeder
Charles Dai

REPORT DOCUMENTATION PAGE

Form Approved
OMB No. 0704-0188

1. REPORT DATE *(DD-MM-YYYY)*	2. REPORT TYPE	3. DATES COVERED *(From - To)*
March 2010	Final	Jan 2009 - Oct 2009

4. TITLE AND SUBTITLE
Numerical Simulation of Propeller Performance with an Inclined Shaft Arrangement

5a. CONTRACT NUMBER

5b. GRANT NUMBER

5c. PROGRAM ELEMENT NUMBER

6. AUTHOR(S)
Seth Schroeder
Charles Dai

5d. PROJECT NUMBER

5e. TASK NUMBER

5f. WORK UNIT NUMBER
09-1-9112-119

7. PERFORMING ORGANIZATION NAME(S) AND ADDRESS(ES) AND ADDRESS(ES)

Resistance and Propulsion Division, Code 5800
Naval Surface Warfare Center Carderock Division
9500 Macarthur Boulevard
West Bethesda, MD 20817-5700

8. PERFORMING ORGANIZATION REPORT NUMBER

NSWCCD-50-TR-2010/024

9. SPONSORING / MONITORING AGENCY NAME(S) AND ADDRESS(ES)
Naval Sea Systems Command,
SEA05D1
Washington Navy Yard
1333 Isaac Hull Avenue, SE
Washington, DC 20376

10. SPONSOR/MONITOR'S ACRONYM(S)
SEA05D

11. SPONSOR/MONITOR'S REPORT NUMBER(S)

12. DISTRIBUTION / AVAILABILITY STATEMENT
Distribution statement A:
Approved for public release. Distribution unlimited.

13. SUPPLEMENTARY NOTES

14. ABSTRACT

A propeller in an inclined shaft arrangement has been simulated using a Reynolds-Averaged Navier-Stokes solver. The commercially available codes Ansys' Fluent and IcemCFD were used for the numerical simulation. The method has been demonstrated through a series of simulations advancing in complexity. The simulations begin with steady-state, single blade calculations and advance to fully unsteady, full 360° domain calculations. Each simulation is supported through comparison with experimental data. This report describes in detail the full process used for the simulation of a propeller. Meshing techniques, solver settings, and post-processing quantities are all examined. Comparisons are made for computational vs. experimental data and for computational data sets at differing conditions. These simulations have demonstrated existing propeller modeling capabilities and further developed capabilities towards the modeling of a ship performing a maneuver. Further study will be conducted by coupling the propeller domain with a rudder domain and examining the interaction between the two components.

15. SUBJECT TERMS
PROPULSOR, HYDRODYNAMICS, RANS

16. SECURITY CLASSIFICATION OF:			17. LIMITATION OF ABSTRACT	18. NUMBER OF PAGES	19a. NAME OF RESPONSIBLE PERSON
UNCLASSIFIED					Seth Schroeder
a. REPORT	b. ABSTRACT	c. THIS PAGE			19b. TELEPHONE NUMBER
UNCLASSIFIED	UNCLASSIFIED	UNCLASSIFIED	SAR	30	(301) 227-5775

(THIS PAGE INTENTIONALLY LEFT BLANK)

CONTENTS

FIGURES

TABLES

NOMENCLATURE

c	Chord length
C_P	Pressure coefficient
D	Diameter
g	Gravitational constant
J_a	Advance coefficient based on inflow velocity
k	Kinetic energy of turbulence
K_Q	Torque coefficient
K_T	Thrust coefficient
N_{CFL}	Courant Number
nb	Number of propeller blades
n	Rotational speed in rotations per second
p	Pressure
Re	Reynolds Number
r	Local radius
s	Distance along chord
t	Thickness
V	Inflow velocity
V_T	Tangential velocity
V_X	Axial velocity
x	Axial coordinate
y	Coordinate normal to a surface
y^+	Non-dimensionalized wall distance
Δ	Change
ε	Dissipation rate of turbulence
η	Open water efficiency
ν	Kinematic viscosity
ρ	Mass density
τ	Shear stress

ABBREVIATIONS

NSWCCD	Naval Surface Warfare Center, Carderock Division
CFD	Computational Fluid Dynamics
RANS	Reynolds-Averaged Navier-Stokes
RPM	Revolutions per minute
IGES	Initial Graphics Exchange Standard

(THIS PAGE INTENTIONALLY LEFT BLANK)

ABSTRACT

A propeller in an inclined shaft arrangement has been simulated using a Reynolds-Averaged Navier-Stokes solver. The commercially available codes Ansys' Fluent and IcemCFD were used for the numerical simulation. The method has been demonstrated through a series of simulations advancing in complexity. The simulations begin with steady-state, single blade calculations and advance to fully unsteady, full 360° domain calculations. Each simulation is supported through comparison with experimental data. This report describes in detail the full process used for the simulation of a propeller. Meshing techniques, solver settings, and post-processing quantities are all examined. Comparisons are made for computational vs. experimental data and for computational data sets at differing conditions. These simulations have demonstrated existing propeller modeling capabilities and further developed capabilities towards the modeling of a ship performing a maneuver. Further study will be conducted by coupling the propeller domain with a rudder domain and examining the interaction between the two components.

ADMINISTRATIVE INFORMATION

Funding for this project was provided by the Cross Platform Systems Development (CPSD) task 6.2 Propulsor Maneuvering Forces under the System Engineering Technical Authority (SETA) project. The project was sponsored by James Webster, NAVSEA 05D1. The work was conducted by the Naval Surface Warfare Center, Carderock Division (NSWCCD), Hydromechanics Department, Resistance and Propulsion Division (Code 5800) under job order number 09-1-9112-119-41.

INTRODUCTION

This report describes the unsteady computational analysis of NSWCCD propeller 4990 with an inclined shaft configuration. The objective of this analysis is to outline a method to perform such calculations and to support the method through rigorous demonstration exercises. This type of analysis provides propeller performance prediction capability by providing a computational analysis tool capable of simulating an unsteady non-axial inflow to a propeller such as is seen by an inclined shaft arrangement or during a maneuver. The objective of this report is to document the computations in as much detail that is required for repeatability in future studies.

The unsteady calculations are supported by a series of increasingly involved Reynolds-Averaged Navier Stokes (RANS) calculations which are detailed below in Figure 1. Each step in this process is compared to experimental data. The tools used for the RANS simulation are commercially available Ansys' IcemCFD [1] and Fluent [2]. As it can be seen in Figure 1, the calculations begin with a single blade passage computation with uniform axial inflow velocity. The cases build on experimental comparison and previous steps to achieve the end results. The fully 5-bladed simulations are conducted for the inclined shaft arrangements. The 5-bladed simulations are carried out in two different ways. The first approach is a quasi-steady approach where the blades are stationary and the blade rotation is introduced by applying a rigid body rotational speed around the propeller axis at the inlet plane. The quasi-steady approach is blade position dependent and it needs to be computed at each blade angle of interest. The second approach is a fully unsteady simulation where the blades are rotating relative to the inertial frame of interest. The experimental data used for comparison are a series of open water tests performed at NSWCCD[1].

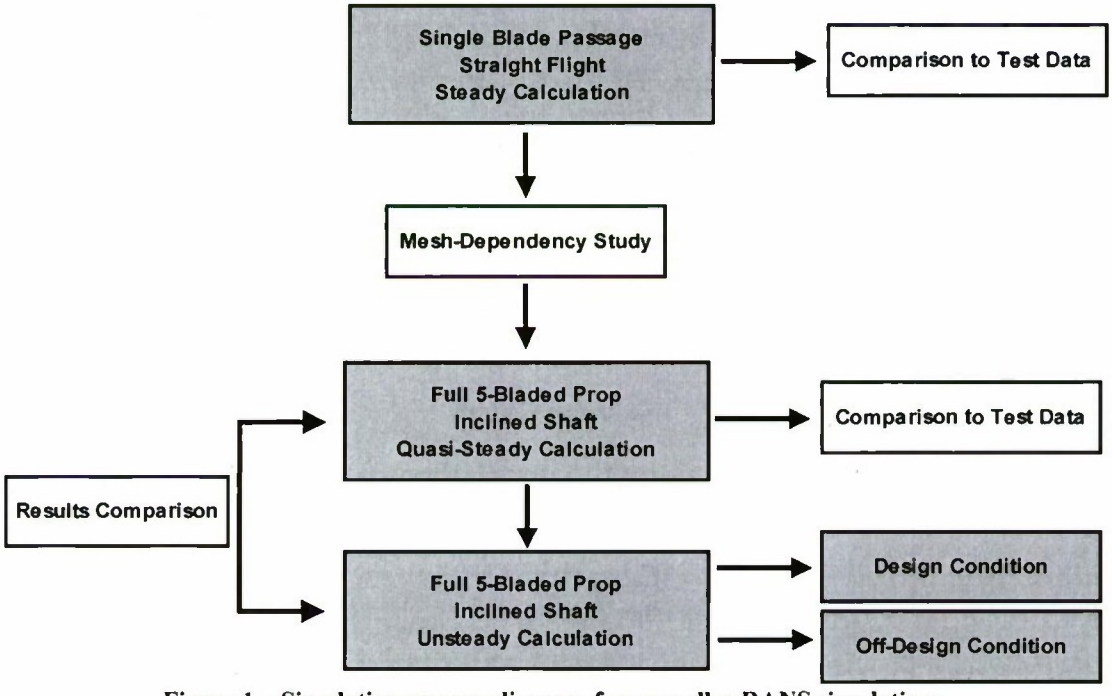

Figure 1 – Simulation process diagram for propeller RANS simulations.

[1] NSWCCD Propeller Library

DOMAIN AND MESHING

All of the meshing was completed using the commercially available Ansys' ICEM CFD [1]. The definition of the boundary geometries (inlet, outlet, periodic, far-field) for the simulation domain were created within ICEM. The blade and hub geometries were imported to ICEM through IGES files. The blade geometry was created using the NSWCCD NURBS surface definition code NCBLADE [3]. The NCBLADE c-array output file is converted to an IGES file, which can be read in by ICEM. The hub geometry was created by converting an axisymmetric curve to a three-dimensional IGES file.

The two separate meshes generated were a single blade passage mesh and a full 360° domain mesh. The particulars for each mesh are described in the following sections. An example illustration of the single blade passage domain can be seen in Figure 2.

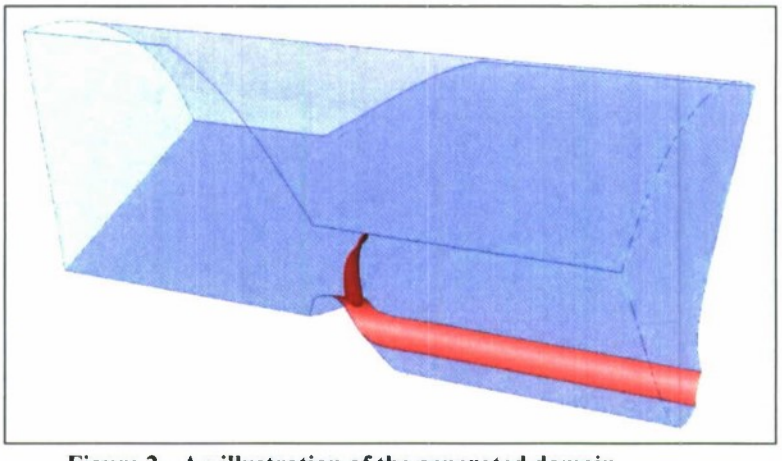

Figure 2 - An illustration of the generated domain.

Every mesh generated for this study contained a structured hexahedral topology scheme. The topology was defined in ICEM using a top-down blocking approach. The type of blocking used was generally H-O type topology. An O-grid was used around the root of the blade, modified with a Y-block at the leading and trailing edges to distinguish between the pressure and suction sides of the blade. An illustration of this O-grid topology with Y-blocks at the leading and trailing edge is seen in Figure 3. An O-grid was also used on the surface of the blade to improve cell quality in critical areas. An illustration of the O-grid on the blade surface is seen in Figure 4.

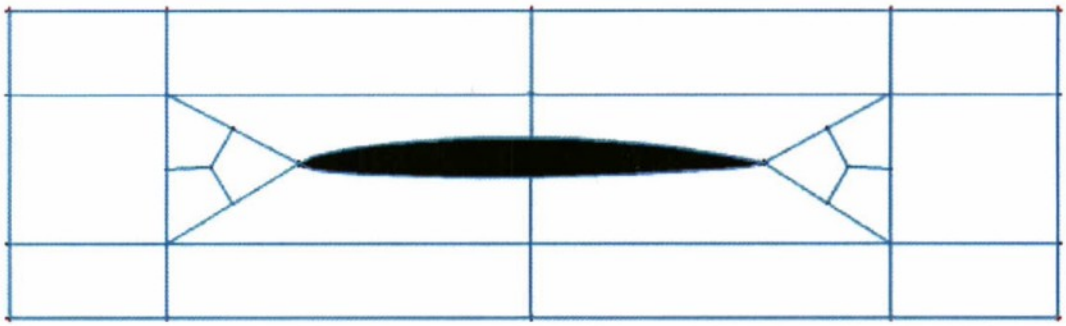

Figure 3 - An illustration of O-grid topology with Y-blocks at the leading and trailing edge of the blade.

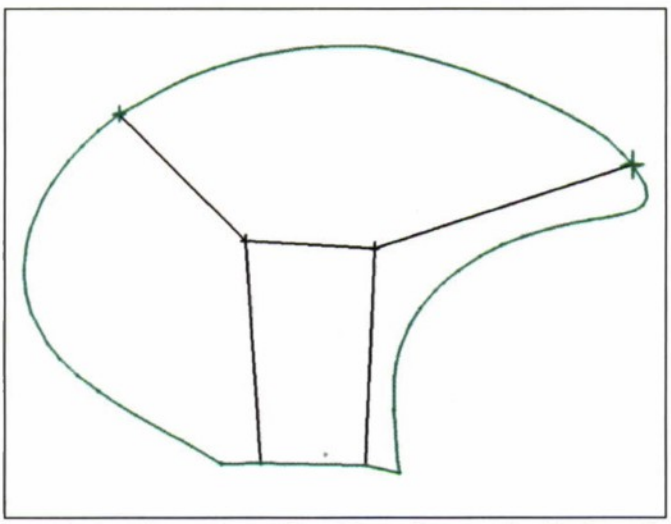

Figure 4 - An illustration of O-grid topology on the blade surface.

The turbulence model used for the simulations was the k- ε turbulence model. This turbulence model includes terms for turbulent kinetic energy, k, and turbulent dissipation rate, ε. The k- ε turbulence model is designed to take advantage of $y+$ values above 30 and wall functions. Fluent uses a two-layer wall model which subdivides the whole domain into a viscosity-affected region and a fully-turbulent region.

Excluding the later mesh independence studies, mesh sizes were designed to leverage wall functions to decrease the number of cells and computing time. The wall spacing was calculated such that the average wall $y+$ value at design condition was 45. This allowed for a wall $y+$ ranging from approximately 25 to 80. This first cell spacing was used on all wall boundaries which included the blades, shaft, and hub. As the spacing of cells off the wall was increased, a geometric growth of 1.1 – 1.2 was used. This growth rate defines how large each cell can be as distance from the wall increases. For example, if a growth rate of 1.1 is used, the

second cell layer is 10% larger than the first cell distance off the wall. The growth rate is used until the cell thickness reaches the prescribed maximum thickness at which point a constant spacing is used. Wall $y+$ is defined as:

$$y^+ = \frac{\rho u_\tau y}{\mu} \qquad (1)$$

where y = distance to the wall, u_τ = friction velocity, ρ = density, and μ = dynamic viscosity.

Axially, the domain extended $2*D$ upstream of the blade and $2*D$ downstream of the blade, where D is the propeller diameter. Radially, the domain extended $1.5*D$ from the root of the blade, or $1*D$ from the tip.

SINGLE BLADE PASSAGE MESH

The solution time for a steady-state computation can be significantly decreased by taking advantage of rotational periodicity. A single blade passage can simulate the entire domain if the flow is constrained to be cyclic at the periodic boundaries, which are spaced rotationally at constant ($360/nb$) spacing, where nb is the number of propeller blades.

In a conformal, matching periodic structured mesh, the nodes along the periodic boundaries align with one another. If a node on one periodic boundary is rotated by the periodic angle about the rotating axis, a corresponding matching node is found on the other periodic boundary. For a modern propeller application this presents a problem. The pitch angle of the blade is such that an extreme angle is created between the chord of the blade and the periodic rotation axis. This extreme angle leads to highly skewed elements in the mesh, which causes difficulties with convergence and stability in the solution process. An example of matching periodic boundaries with a 2D cross section of a blade is seen in Figure 5. In the figure, it can be seen that nodes matching cyclically about the x-axis cause extreme angles relative to the blade near the blade surface.

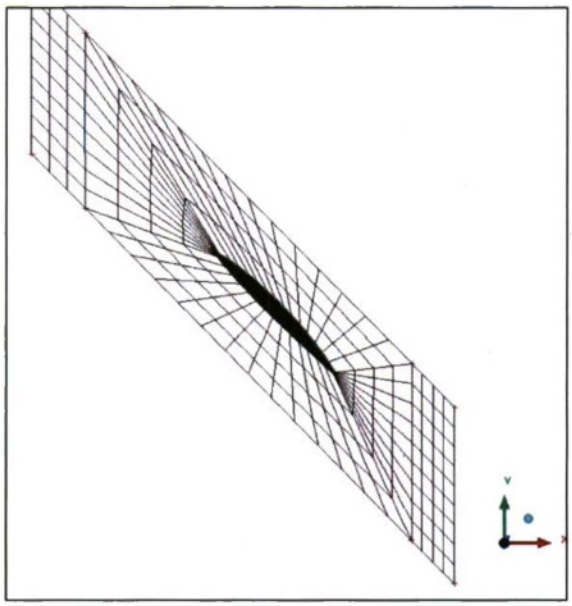

Figure 5 - Example of matching periodic boundaries.

To correct the extreme angles caused by matching periodic boundaries, an interpolation method can be used on the periodic boundaries. This interpolation allows for non-matching nodes on the periodic boundaries. In general, the error introduced through the interpolation method is insignificant when compared to the error and convergence problems that can be caused by a highly skewed mesh. An example of this preferred method of non-matching periodic boundaries can be seen in Figure 6.

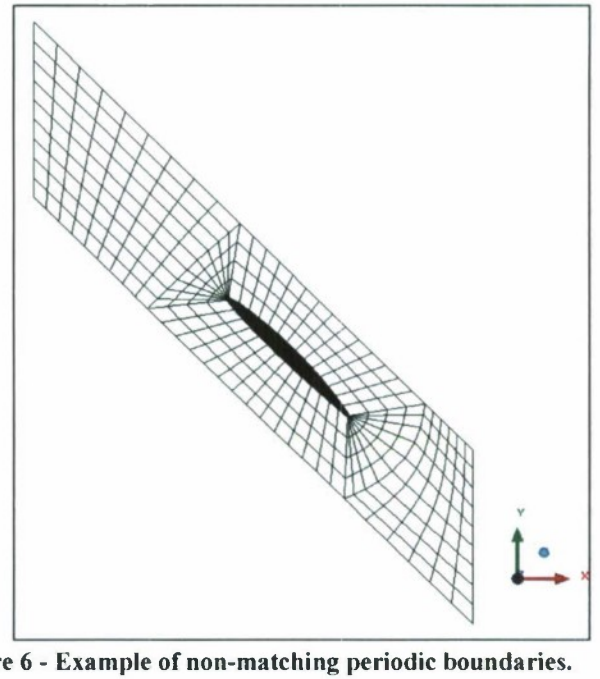

Figure 6 - Example of non-matching periodic boundaries.

The mesh was manually refined to meet two primary quality criteria, the minimum cell angle, and the 2x2x2 determinant. The minimum cell angle is determined by the smallest internal angle of an element. An angle of 90 indicates a perfectly cubic element and an angle of 0 indicates a degenerate element. The 2x2x2 determinant is a measure of skewness of the cell and it is defined as the ratio of the smallest determinant of the Jacobian matrix divided by the largest determinant of the Jacobian matrix. A 2x2x2 determinant of 1 indicates a perfectly regular element. A determinant of 0 or less indicates an element which has a degenerate edge or is inverted. Because mesh quality impacts solution stability and accuracy, the minimum internal angle was to be above 18 degrees and the smallest 2x2x2 determinant was to be above 0.4. The mesh was manually refined until both of these conditions were satisfied. The resulting single blade passage mesh contained 1 million hexahedral cells.

FULL 5-BLADED PROPELLER MESH

To complete the transient cases of the study, a full 360-degree domain of all 5 propeller blades was needed. This was created by copying the original single passage mesh rotationally. Because the nodes were non-matching on the periodic interfaces, an interpolation was still needed between the blades. Again, the interpolation scheme was preferable to the conforming boundaries which introduced error by the highly skewed cells. An illustration of the full 360-

degree mesh can be seen in Figure 7. In this figure, each rotational copy differs in color to exemplify the non-conformal boundaries.

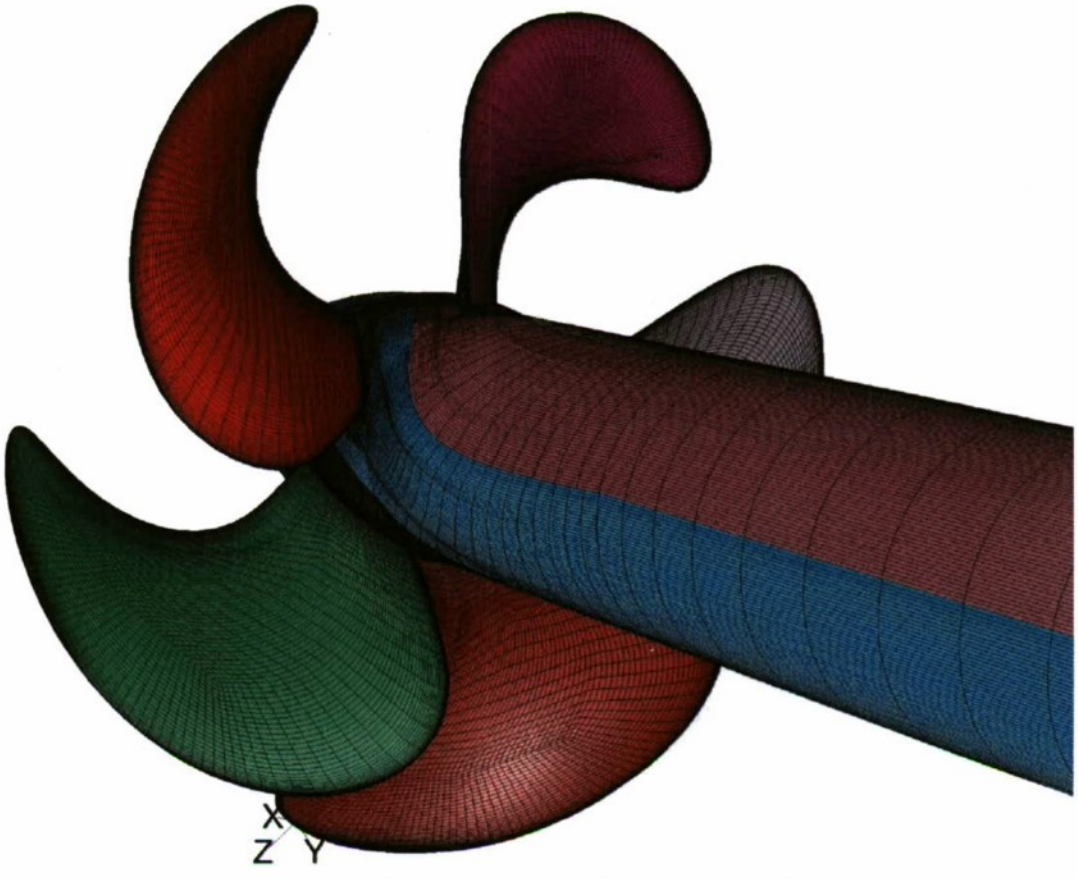

Figure 7 – An illustration of the full 360-degree mesh.

SINGLE BLADE PASSAGE SOLUTION PROCESS AND RESULTS

The first step in demonstrating the RANS process was to compare with the open water test results. This was done by using a single blade passage mesh with a steady state solver. The commercially available CFD code Fluent [2] was used as the solver for all of the calculations in this study.

The inlet of the domain was prescribed as a velocity-inlet boundary condition. Fluent uses the specified velocity vector to calculate a mass flow into the domain and the corresponding momentum flux through the boundary. The velocity for the straight flight case was always set in the axial direction. The magnitude was varied to achieve simulation conditions for a range of advance coefficient conditions. Advance coefficient is defined as:

$$J_a = \frac{V}{nD} \qquad (2)$$

Where V = inlet velocity, n = rotations per second of the propeller, and D = propeller diameter. The Reynold's number for the simulations was on the order of 1-2 million which matches the experimental data the simulations are later compared to.

The outlet of the domain was prescribed as a pressure-outlet boundary condition. At this boundary the user specifies a static pressure, which was set as equal to the reference pressure of the domain. The far-field boundary condition was set as a slip free-stream condition.

The initial solution was started with low under-relaxation factors set for all parameters. This condition corresponds to an extremely damped system which is very stable during the beginning iterations. Once the first advance coefficient condition was converged, its solution was used as the initial condition for the subsequent advance coefficients. This procedure allowed for a more stable and faster calculation of the open water curve.

The open water curve for a single blade passage solution in straight flight can be seen in Figure 8. As seen, the Fluent results are compared to two separate sets of open water test data. Both tests were conducted at NSWCCD with the same sized model scale propeller.

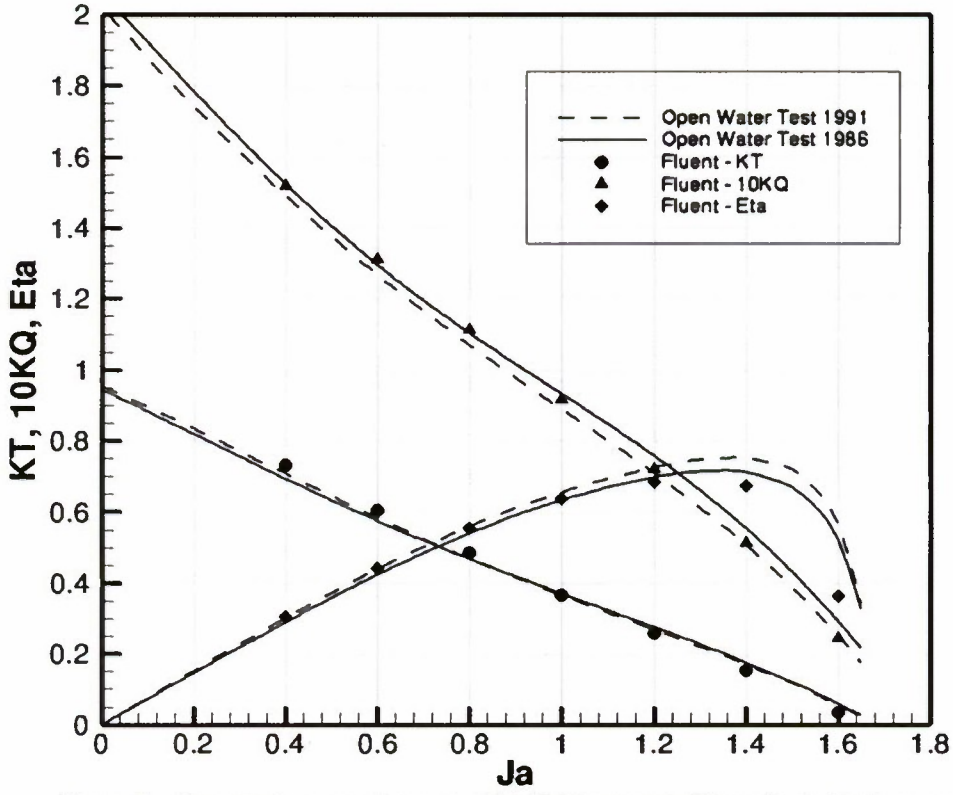

Figure 8 - Open water curve for a straight flight computed by a single blade passage.

In Figure 8, the advance coefficient, J_a, as defined in (2) is compared against the thrust coefficient, K_T, ten times the torque coefficient, $10*K_Q$, and the open water efficiency, η. The three dependent variables are defined as:

$$K_T = \frac{Thrust}{\rho n^2 D^4} \tag{3}$$

$$K_Q = \frac{Torque}{\rho n^2 D^5} \tag{4}$$

$$\eta = \frac{J_a K_T}{2\pi K_Q} \tag{5}$$

where ρ = density, n = rotations per second of the propeller, and D = propeller diameter. The force values are computed by integrating forces on only the blade surfaces, and do not include the shaft and hub.

It can be seen in Figure 8 that good agreement was achieved for uniform inflow conditions. It can be seen that the thrust and torque are both slightly over predicted at an advance coefficient less than 1 and slightly under predicted at an advance ratio above 1.0. These results can be seen in tabular form in Tables 1 through 3 where the results are compared to the average

value of the two experiments. In the tables, the percent difference is shown as the absolute difference of the calculation relative to the experiment. The main difference between the simulations and the experiments is the shaft location. In the simulations an upstream shaft is used to more closely mimic actual ship operating conditions. The experiments are driven with a downstream shaft to simulate true open water conditions, leaving a difference between the two in that there is no boundary layer being introduced to the propeller inflow in the experimental setup.

Table 1 - Open water thrust coefficients for straight flight.

K_T			
J	Experiment	Calculation	Difference
0.400	0.701	0.732	4.50%
0.600	0.580	0.607	4.71%
0.800	0.469	0.486	3.61%
1.000	0.369	0.367	0.30%
1.200	0.273	0.258	5.37%
1.400	0.174	0.155	10.98%

Table 2 - Open water torque coefficients for straight flight.

$10K_Q$			
J	Experiment	Calculation	Difference
0.400	1.507	1.525	1.22%
0.600	1.282	1.316	2.67%
0.800	1.086	1.116	2.77%
1.000	0.911	0.918	0.87%
1.200	0.734	0.723	1.47%
1.400	0.531	0.513	3.21%

Table 3 - Open water efficiency for straight flight.

Open Water Efficiency			
J	Experiment	Calculation	Difference
0.400	0.296	0.306	3.21%
0.600	0.432	0.440	1.97%
0.800	0.550	0.554	0.79%
1.000	0.644	0.637	1.20%
1.200	0.711	0.683	4.02%
1.400	0.732	0.672	8.14%

MESH INDEPENDENCE

If a mesh is of sufficient resolution for a given problem, the results will not differ even when a finer mesh is considered. Proving that a mesh is of sufficient resolution is called mesh

independence evaluations. This condition is established through a series of differing mesh resolutions in which the mesh size is altered globally.

Additionally, the extent of the domain can impact the solution. That is, how far the domain extends upstream, downstream, and radially. Previously, Rhee and Joshi [4] demonstrated that an extended domain $2*D$ downstream gave the same results as a domain that extended only $0.72*D$ downstream. As previously stated, the domain used for this study did extend $2*D$ downstream, so dependency on domain extent was not studied.

For this simulation, the mesh size was effectively doubled. To double the global size of the mesh, the element count was increased by a factor of $2^{1/3}$ in each direction. Meaning that there are $2^{1/3}$ more elements in the x, y, and z directions, which when applied to the volume effectively doubles the total element count. This grid resolution brought the total cell count to approximately 2 million hexahedral elements. A uniform inflow open water performance curve was calculated in exactly the same manner by analyzing approximately the same range of advance coefficients. The results of these calculations can be seen compared against the original mesh in Figure 9. The two different meshes gave very similar results. The only outlier seems to occur at an advance coefficient of $J_a = 0.6$ which is an off-design condition. Even though this point shows slight disagreement between the two meshes, the torque seems to be the coefficient with the largest discrepancy, and it varies by only 1.8%. It was therefore concluded that the proceeding simulations were mesh independent.

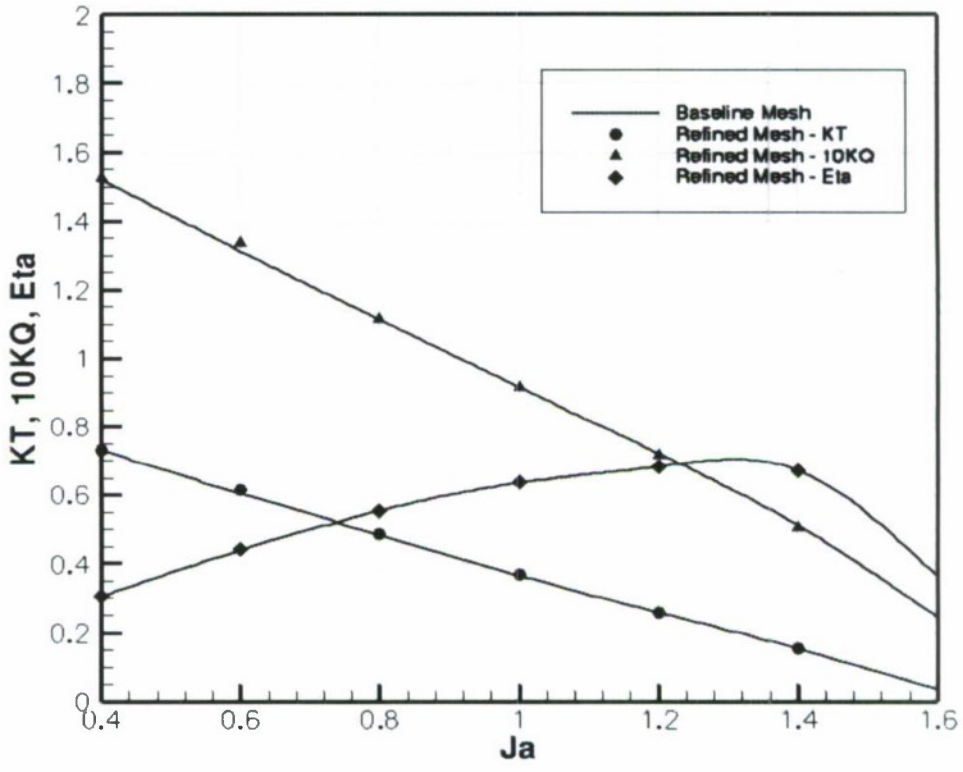

Figure 9 - Mesh dependency study open water results.

FULL 5-BLADED PROPELLER SOLUTION PROCESS AND RESULTS

With the comparison of open water test data and grid independence established, the next step was to demonstrate an inclined shaft assembly. The computational method used to simulate the inclined shaft arrangement is very similar to the proposed method for cross-flow. Therefore, the demonstrated method can be used for any subsequent cross-flow simulations in the future. However, a single blade passage mesh is inadequate to simulate an inclined shaft arrangement or a cross-flow because any non-axial component of velocity prescribed at the inlet of the domain will be rotated as the domain is cyclically copied by the solver.

The use of a full 360 degree domain allows for an inflow containing non-axial velocities to be studied. By simply adding a vertical component of velocity, the same mesh can be used to simulate any shaft angle and/or cross-flow angle. For an inclined shaft, the components of the inflow were defined as:

$$V_x = V\cos(shaft\ angle) \quad (6)$$

$$V_y = V\sin(shaft\ angle) \quad (7)$$

Test data were available for two open water tests with different inclined shaft angles. This allowed for the comparison of inflows with a non-axial component. Two different approaches were studied in this phase of this simulation. The first approach was a quasi-steady approximation in which the rotating reference frame model was leveraged. The second approach was to complete a fully transient simulation with the mesh rotating relative to the inertial frame.

The steady-state solution of a rotating propeller is possible by transforming the fluid velocities from the stationary frame to the rotating frame by introducing a relative velocity which includes the velocity due to the moving of the reference frame. With an inclined shaft, the angle of attack of each individual blade as well as its position in the wake of the shaft varies as a function of time as the propeller rotates. Completing a quasi-steady simulation only allows for a snapshot in time of the propeller performance. This limitation means that any quantity with a strong transient behavior will not be properly captured in the quasi-steady solution. In the following pages the simulations for the quasi-steady solutions are compared against the fully unsteady solutions.

QUASI-STEADY RESULTS

The quasi-steady solution offers a look at a single moment in time of an unsteady system. It can be compared to the instantaneous results of a given experiment rather than a time sampling.

The quasi-steady calculations consisted of a range of advanced ratios adequate for an open water curve. These calculations were run for both of the two inclined shaft angles that were tested at NSWCCD, 4.8 degrees and 8.8 degrees. The Fluent results compared against the experimental data for the 4.8 degree inclined shaft angle can be seen in Figure 10. These results can be seen in tabular form in Tables 4 through 6.

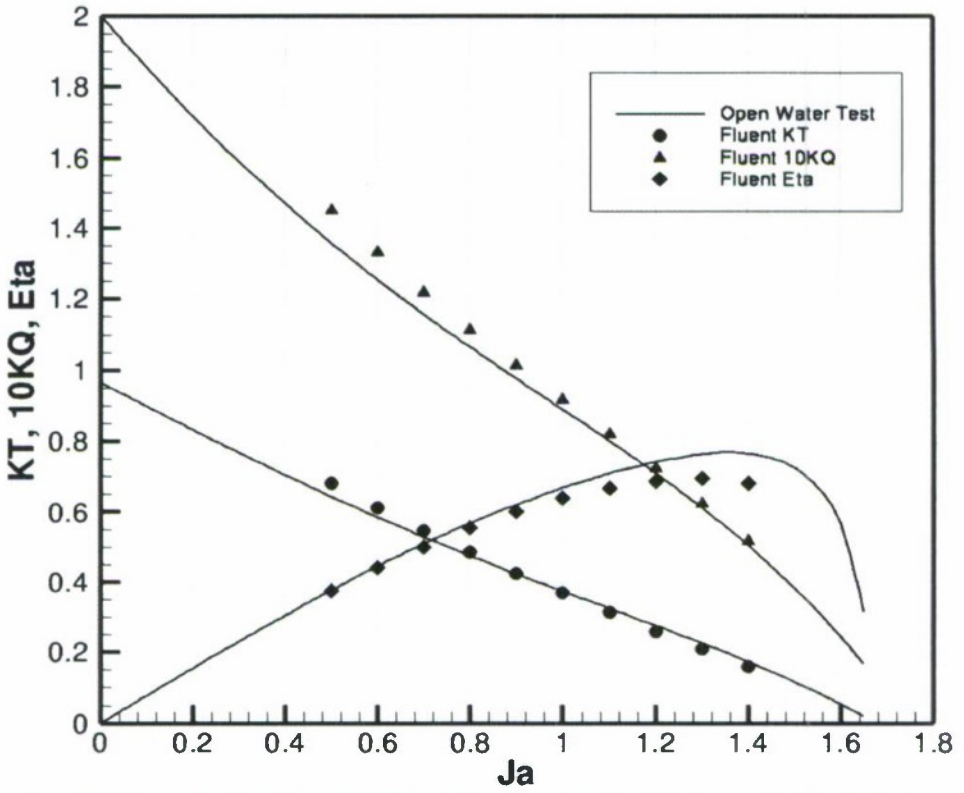

Figure 10 – Quasi-steady Fluent vs. experimental open water results for an inclined shaft angle of 4.8°.

Table 4 - Thrust coefficient values for an inclined shaft angle of 4.8°.

K_T			
J	Experiment	Calculation	Difference
0.400	0.704	0.739	5.02%
0.500	0.643	0.681	5.91%
0.600	0.585	0.613	4.75%
0.700	0.528	0.547	3.63%
0.800	0.475	0.485	2.04%
0.900	0.423	0.425	0.49%
1.000	0.374	0.368	1.62%
1.100	0.325	0.313	3.66%
1.200	0.276	0.260	5.62%
1.300	0.226	0.209	7.44%
1.400	0.173	0.158	8.85%

Table 5 - Torque coefficient values for an inclined shaft angle of 4.8°.

$10K_Q$			
J	Experiment	Calculation	Difference
0.400	1.468	1.554	5.85%
0.500	1.356	1.450	6.95%
0.600	1.253	1.331	6.22%
0.700	1.156	1.218	5.40%
0.800	1.065	1.113	4.54%
0.900	0.976	1.013	3.83%
1.000	0.889	0.916	3.08%
1.100	0.801	0.820	2.39%
1.200	0.71	0.724	1.91%
1.300	0.612	0.623	1.82%
1.400	0.504	0.515	2.25%

Table 6 - Open water efficiency values for an inclined shaft angle of 4.8°.

Open Water Efficiency			
J	Experiment	Calculation	Difference
0.400	0.305	0.303	0.78%
0.500	0.377	0.374	0.97%
0.600	0.446	0.440	1.38%
0.700	0.509	0.500	1.68%
0.800	0.568	0.554	2.40%
0.900	0.621	0.601	3.21%
1.000	0.670	0.639	4.56%
1.100	0.710	0.668	5.91%
1.200	0.742	0.688	7.39%
1.300	0.764	0.695	9.09%
1.400	0.765	0.682	10.86%

The calculations are once again in good agreement with the experimental data. It can be noted that both the thrust and torque values are predicted slightly high at lower off-design advance coefficients for the 4.8° inclined shaft arrangement. The torque values remain slightly high throughout the range while the thrust values shift from over prediction to under prediction around an advance coefficient of 1.0.

The Fluent calculations compared against the experimental data for an 8.8° inclined shaft arrangement can be seen below in Figure 11. These results can also be seen in tabular form in Tables 7 through 9.

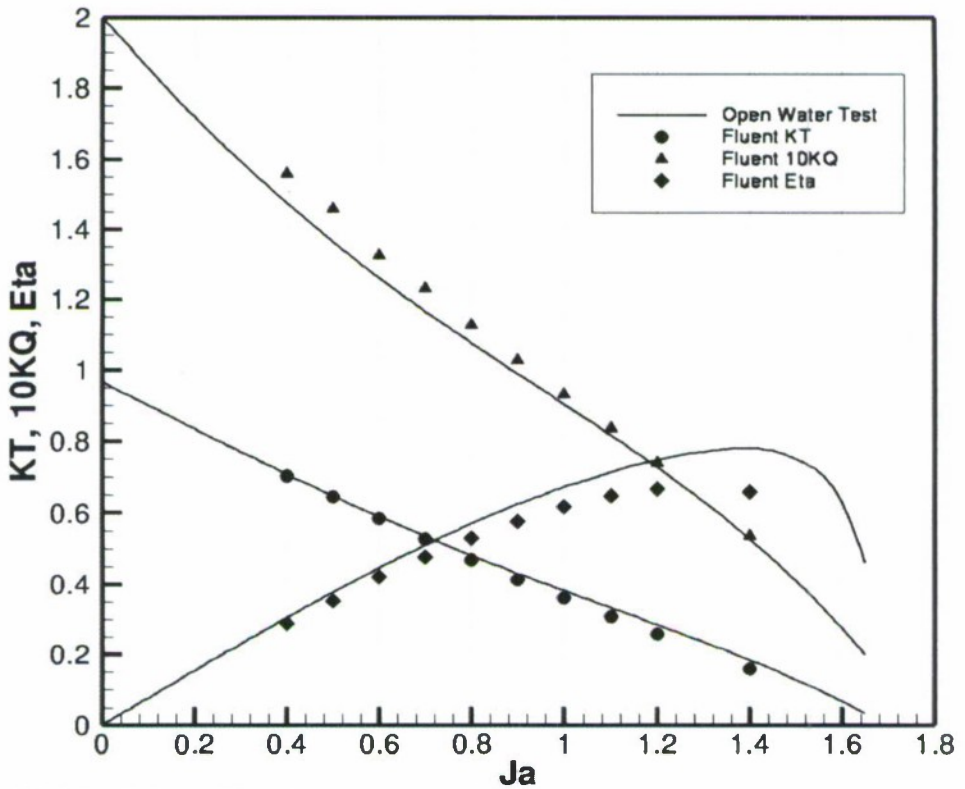

Figure 11 – Quasi-steady Fluent vs. experimental open water results for an inclined shaft angle of 8.8°.

Table 7 - Thrust coefficient values for an inclined shaft angle of 8.8°.

K_T			
J	Experiment	Calculation	Difference
0.400	0.708	0.704	0.53%
0.500	0.648	0.645	0.40%
0.600	0.590	0.585	0.88%
0.700	0.534	0.526	1.41%
0.800	0.481	0.469	2.46%
0.900	0.431	0.414	3.96%
1.000	0.382	0.361	5.52%
1.100	0.333	0.309	7.30%
1.200	0.285	0.258	9.37%
1.400	0.185	0.158	14.79%

Table 8 - Torque coefficient values for an inclined shaft angle of 8.8°.

$10K_Q$			
J	Experiment	Calculation	Difference
0.400	1.474	1.557	5.62%
0.500	1.364	1.457	6.81%
0.600	1.261	1.324	4.96%
0.700	1.166	1.232	5.66%
0.800	1.075	1.127	4.79%
0.900	0.988	1.027	3.97%
1.000	0.903	0.931	3.15%
1.100	0.817	0.835	2.23%
1.200	0.728	0.740	1.62%
1.400	0.528	0.534	1.12%

Table 9 - Open water efficiency values for an inclined shaft angle of 8.8°.

Open Water Efficiency			
J	Experiment	Calculation	Difference
0.400	0.306	0.288	5.82%
0.500	0.378	0.353	6.74%
0.600	0.447	0.422	5.57%
0.700	0.510	0.476	6.69%
0.800	0.570	0.530	6.92%
0.900	0.625	0.577	7.63%
1.000	0.673	0.617	8.41%
1.100	0.714	0.647	9.33%
1.200	0.748	0.667	10.82%
1.400	0.781	0.658	15.74%

The results for the 8.8° inclined shaft are very similar to those of the previously discussed 4.8° case. Once again the torque is over-predicted throughout the entire range of advance coefficients. However, the thrust values seem to be simply under predicted at an advance

coefficient higher than 0.8 rather than being over predicted in the lower advance coefficient range.

FULLY UNSTEADY RESULTS

The unsteady calculations were stably run at Courant numbers of approximately 20. Courant number (CFL number) is defined as:

$$CFL = \frac{u\,\Delta t}{\Delta x} \qquad (8)$$

where u = velocity, Δt = time step size, and Δx = grid spacing. This translated into approximately 1 degree of rotation per time step. The solutions converged quickly and once a solution was achieved a time step could be completed in approximately 0.5-1 hour using 6-8 parallel cores of a dual Intel Xeon 3.0GHz processor machine.

Fully unsteady calculations were done at both shaft angles. The 8.8° case was run at an advance ratio of J_a=1.2, which was close to the design condition. The 4.8° case was run at an off design advance ratio of J_a=0.4. The comparison between quasi-steady and fully unsteady results can be seen in Tables 10 and 11. In the tables, the percent difference is shown as the quasi-steady relative to unsteady results. It can be seen that for both cases, the calculated global quantities, K_Q, K_T, and η were all within 1-4% of the values calculated by the quasi-steady calculations for the corresponding conditions. This result suggests that the quasi-steady calculation is adequate for determining the global open water coefficients for an inclined shaft arrangement.

Table 10 - Quasi-steady vs. Unsteady open water coefficients for 8.8° shaft angle, J_a=1.2.

8.8° shaft angle, J_a=1.2			
Case	**K_T**	**$10K_Q$**	**η**
Quasi-Steady	0.258	0.740	0.667
Unsteady	0.268	0.734	0.697
Difference	3.62%	0.79%	4.33%

Table 11 - Quasi-steady vs. Unsteady open water coefficients for 4.8° shaft angle, J_a=0.4.

4.8° shaft angle, J_a=0.4			
Case	**K_T**	**$10K_Q$**	**η**
Quasi-Steady	0.739	1.554	0.303
Unsteady	0.751	1.576	0.303
Difference	1.54%	1.42%	0.12%

While the global quantities did not change as a function of the propellers rotation, locally the force on each blade varied as a function of its position in the flow field. In the fully unsteady calculations, a monitor was able to track this force. This result is illustrated in Figure 12, which

shows the K_T value of an individual blade as it completes a full rotation. The case shown in this plot corresponds to an inclined shaft angle of 4.8° at an off design advance coefficient of 0.4. For comparison purposes, total K_T value is shown on the second y-axis. It can be noted that the thrust of the blade changes approximately +/- 2% during a rotation. Similarly, the torque coefficient, $10K_Q$ is plotted in the same manner for the same case in Figure 13. The torque coefficient shows behavior very similar to the thrust as the blade goes through a full rotation. It can be noted that the other blades vary identically to the one blade shown and would simply include a phase shift of 360° / number of blades = 72° if plotted on the same axis.

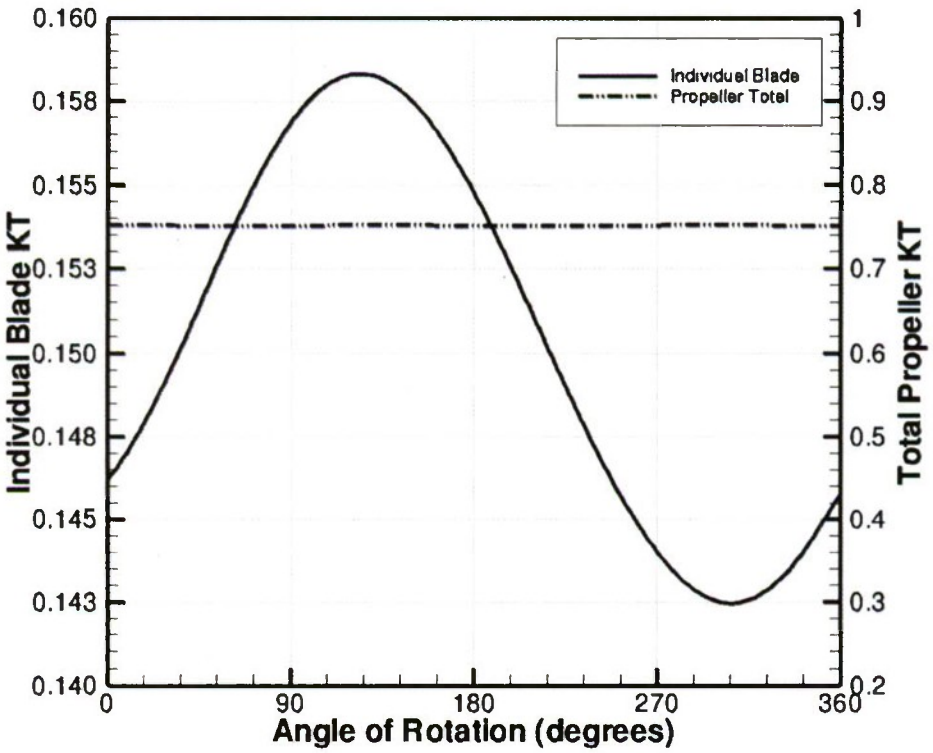

Figure 12 - K_T of an individual blade during a single rotation for an inclined shaft of 4.8° and J_a=0.4.

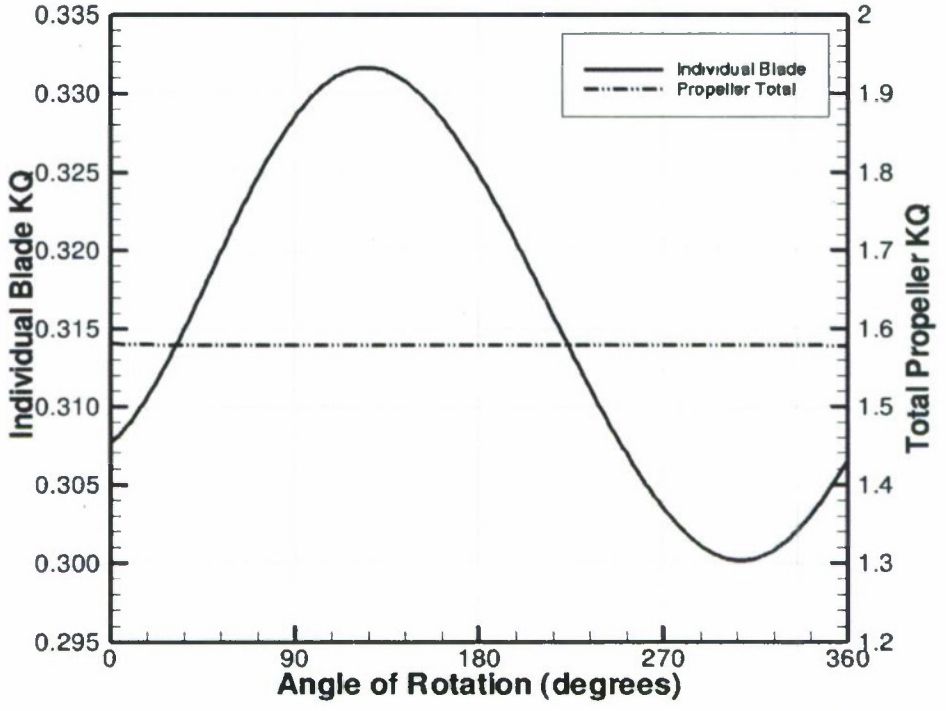

Figure 13 - K_Q of an individual blade during a single rotation for an inclined shaft of 4.8° and J_a=0.4.

The impact of the inclined shaft vs. pure axial inflow can be seen in more detail by examining the pressure contours qualitatively on the blade surface. This also allows a more detailed comparison of steady, quasi-steady, and fully unsteady flow. These comparisons can be seen on the following pages in Figure 14 and Figure 15.

In the figures, the pressure coefficient, C_p, is defined as:

$$C_p = \frac{p}{\frac{1}{2}\rho V^2} \qquad (9)$$

where p = static pressure, and V = ship speed.

In both figures the shaft is inclined in the positive y-direction. This means that the wake of the shaft will be in the top dead center portion of the 360° view. The pressure side contours, shown in Figure 14, show an upstream facing view, meaning that propeller rotation is occurring clockwise in the figure. The suction side contours, shown in Figure 14, show a downstream facing view, meaning that propeller rotation is occurring counter-clockwise in the figure.

It can be seen that the wake of the shaft has a large impact on the quasi-steady cases. The blades that have rotated just out of the wake of the shaft show a large decrease in pressure on the surfaces. While this effect can also be seen in the unsteady case, it is seen to a much lesser extent than in the quasi-steady case. It can also be seen that the blades seem to recover to a higher

pressure just before entering the wake of the shaft for the inclined shaft cases. This result again is much more prevalent in the quasi-steady case.

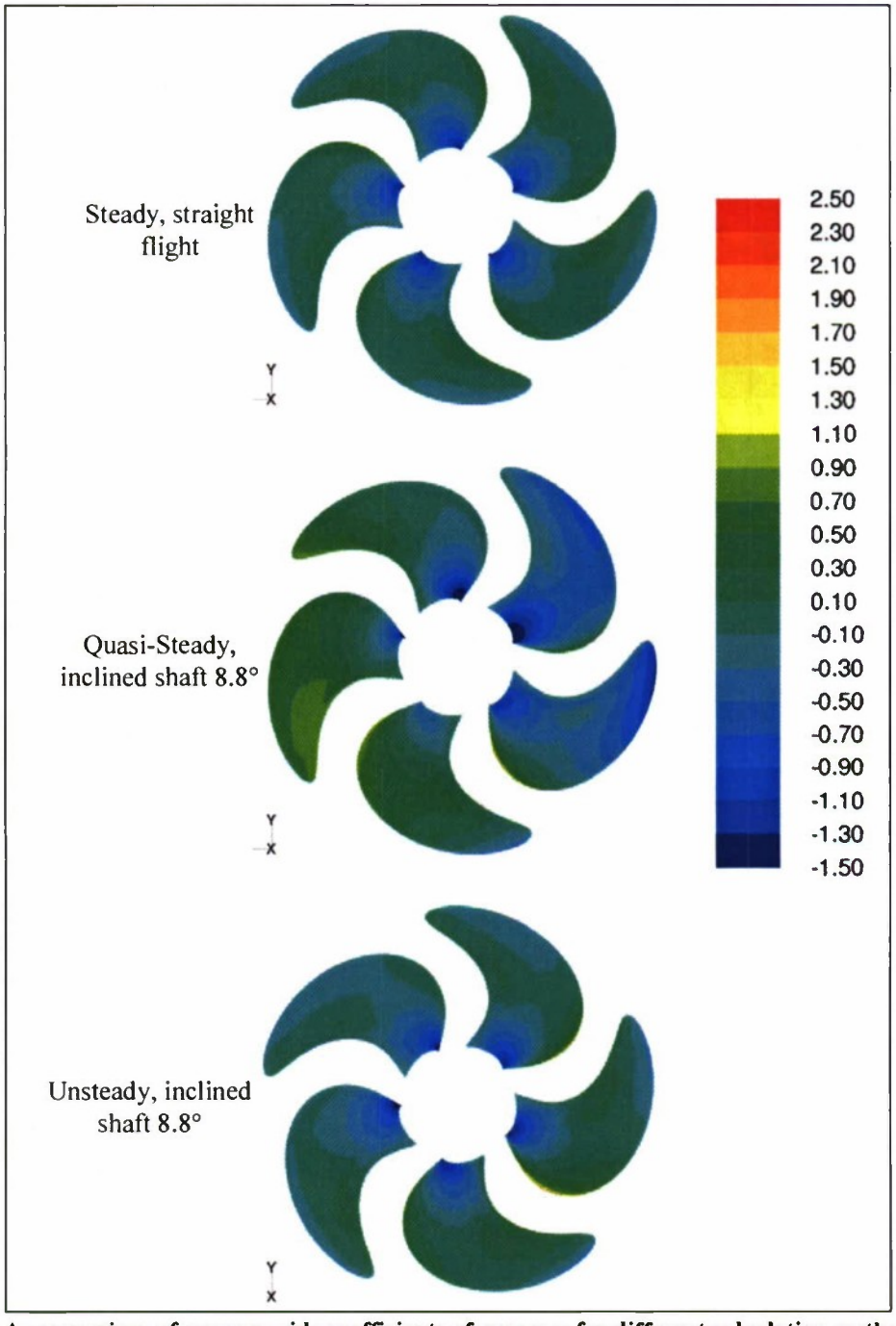

Figure 14 - A comparison of pressure side coefficients of pressure for different calculation methods with an inclined shaft of 8.8° , J_a=1.2.

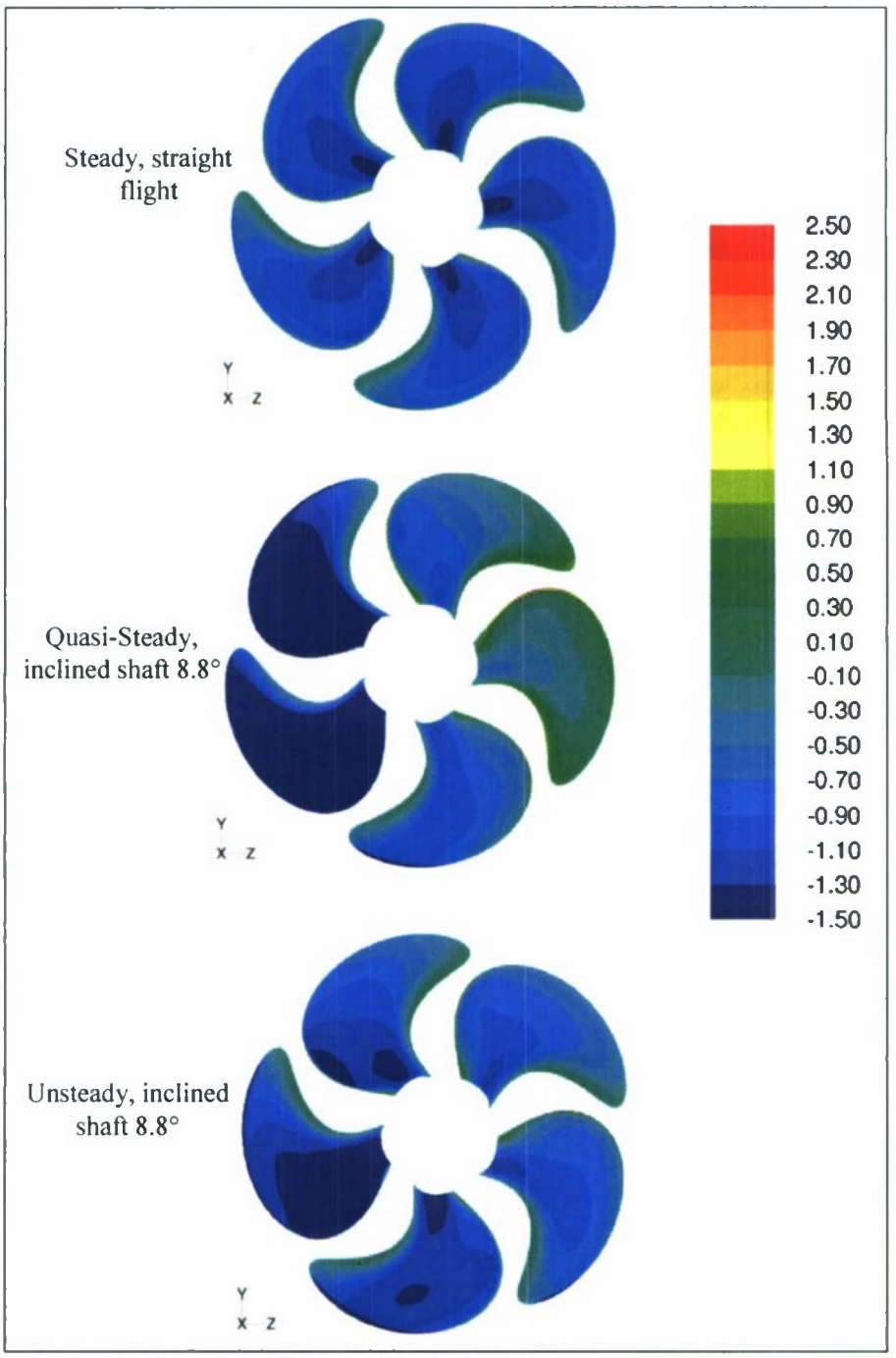

Figure 15 - A comparison of suction side coefficients of pressure for different calculation methods with an inclined shaft of 8.8°, J_a=1.2.

CONCLUSIONS AND RECOMMENDATIONS

A computational method for predicting the performance of a propeller in an inclined shaft arrangement has been demonstrated. This model can be used as a critical piece of an overall ship performance prediction for propulsion, seakeeping, and maneuvering during the design and/or analysis process of current and future Navy ships.

For open water calculations, a single blade passage simulation produced sufficiently accurate results. When applicable, this approach saves time and computational expense by taking advantage of the periodicity of the problem. When an inclined shaft arrangement is desired, a full 360° solution is required. If only the open water coefficients are desired for a similar problem, a quasi-steady analysis can be used to save computation time in certain cases. The quasi-steady analysis seems to have acceptable mean values for the global coefficients; however a large difference can be seen when examining local quantities such as pressure contours on the blade surface. Further cases must be examined to prove the method. The quasi-steady approach looks at a single instance rather than a time sampling. To compare with experimental data that has been sampled in time, and unsteady approach must still be used.

The next step planned for this study is to examine the interaction between the propeller and a rudder as well as to subject the system to a cross-flow. For this planned analysis, the currently demonstrated propeller model will be combined with a validated rudder model through a sliding mesh interface. This simulation will allow correlation between propeller forces and rudder forces subjected to a cross-flow during ship manuevers.

A more detailed comparison of propeller wakes with and without a cross-flow component is also planned. This comparison will reveal the differences in the flow that the rudder is being subject to while the ship is completing a maneuver.

Possible future work includes a more in depth study on the propeller mesh. The large up-front time commitment in making a mesh gives motivation for this work. This study would include a detailed comparison between structured and unstructured mesh types as well as each type's strengths and limitations.

The demonstrated approach using RANS simulation can be used to guide the development of reduced order models for propeller and propeller/rudder flow. One area of ongoing investigation is to provide guidance in the development of propeller wake modeling using potential flow models.

APPENDIX A: OPEN WATER DATA

Table 12 - Open water data for 0° shaft angle, 1991.

Open Water Test 5/1/91			
Shaft Angle = 0°			
J	K_T	$10K_Q$	η
0.000	0.955	2.021	0.000
0.050	0.926	1.949	0.038
0.100	0.897	1.879	0.076
0.150	0.866	1.810	0.114
0.200	0.835	1.743	0.152
0.250	0.803	1.677	0.191
0.300	0.771	1.613	0.228
0.350	0.739	1.551	0.265
0.400	0.708	1.490	0.303
0.450	0.676	1.432	0.338
0.500	0.645	1.375	0.373
0.550	0.614	1.320	0.407
0.600	0.584	1.267	0.440
0.650	0.554	1.215	0.472
0.700	0.525	1.165	0.502
0.750	0.497	1.117	0.531
0.800	0.470	1.069	0.560
0.850	0.443	1.023	0.586
0.900	0.417	0.978	0.611
0.950	0.391	0.933	0.634
1.000	0.366	0.889	0.655
1.050	0.342	0.845	0.676
1.100	0.317	0.800	0.694
1.150	0.293	0.755	0.710
1.200	0.269	0.709	0.725
1.250	0.245	0.661	0.737
1.300	0.221	0.612	0.747
1.350	0.196	0.561	0.751
1.400	0.171	0.507	0.752
1.450	0.144	0.449	0.740
1.500	0.117	0.388	0.720
1.550	0.087	0.323	0.664
1.600	0.056	0.253	0.564
1.650	0.023	0.177	0.341

Table 13 - Open water data for 0° shaft angle, 1986.

Open Water Test 3/4/86			
Shaft Angle = 0°			
J	K_T	$10K_Q$	η
0.000	0.944	2.057	0.000
0.050	0.914	1.990	0.037
0.100	0.883	1.922	0.073
0.150	0.851	1.853	0.110
0.200	0.820	1.785	0.146
0.250	0.788	1.717	0.183
0.300	0.756	1.651	0.219
0.350	0.724	1.586	0.254
0.400	0.693	1.523	0.290
0.450	0.663	1.463	0.325
0.500	0.633	1.405	0.359
0.550	0.604	1.349	0.392
0.600	0.575	1.296	0.424
0.650	0.547	1.244	0.455
0.700	0.520	1.195	0.485
0.750	0.494	1.148	0.514
0.800	0.468	1.103	0.540
0.850	0.443	1.059	0.566
0.900	0.419	1.016	0.591
0.950	0.395	0.974	0.613
1.000	0.371	0.932	0.634
1.050	0.347	0.890	0.652
1.100	0.324	0.847	0.670
1.150	0.300	0.803	0.684
1.200	0.277	0.758	0.698
1.250	0.253	0.711	0.708
1.300	0.228	0.661	0.714
1.350	0.203	0.609	0.716
1.400	0.177	0.554	0.712
1.450	0.149	0.495	0.695
1.500	0.121	0.432	0.669
1.550	0.091	0.365	0.615
1.600	0.060	0.293	0.521
1.650	0.027	0.217	0.327

Table 14 - Open water for 8.8° shaft angle.

Open Water Test			
Shaft Angle = 8.8°			
J	K_T	$10K_Q$	η
0.000	0.966	2.000	0.000
0.050	0.933	1.927	0.039
0.100	0.901	1.855	0.077
0.150	0.868	1.786	0.116
0.200	0.835	1.719	0.155
0.250	0.803	1.655	0.193
0.300	0.771	1.592	0.231
0.350	0.740	1.532	0.269
0.400	0.708	1.474	0.306
0.450	0.678	1.418	0.342
0.500	0.648	1.364	0.378
0.550	0.618	1.312	0.412
0.600	0.590	1.261	0.447
0.650	0.562	1.213	0.479
0.700	0.534	1.166	0.510
0.750	0.508	1.120	0.541
0.800	0.481	1.075	0.570
0.850	0.456	1.032	0.598
0.900	0.431	0.988	0.625
0.950	0.406	0.946	0.649
1.000	0.382	0.903	0.673
1.050	0.357	0.861	0.693
1.100	0.333	0.817	0.714
1.150	0.310	0.773	0.734
1.200	0.285	0.728	0.748
1.250	0.261	0.681	0.762
1.300	0.236	0.633	0.771
1.350	0.211	0.582	0.779
1.400	0.185	0.528	0.781
1.450	0.158	0.471	0.774
1.500	0.129	0.410	0.751
1.550	0.100	0.345	0.715
1.600	0.068	0.275	0.630
1.650	0.035	0.200	0.460

Table 15 - Open water data for 4.8° shaft angle.

Open Water Test			
Shaft Angle = 4.8°			
J	K_T	$10K_Q$	η
0.000	0.966	2.001	0.000
0.050	0.933	1.926	0.039
0.100	0.899	1.854	0.077
0.150	0.866	1.784	0.116
0.200	0.833	1.716	0.155
0.250	0.800	1.650	0.193
0.300	0.768	1.587	0.231
0.350	0.736	1.526	0.269
0.400	0.704	1.468	0.305
0.450	0.674	1.411	0.342
0.500	0.643	1.356	0.377
0.550	0.614	1.304	0.412
0.600	0.585	1.253	0.446
0.650	0.556	1.204	0.478
0.700	0.528	1.156	0.509
0.750	0.501	1.110	0.539
0.800	0.475	1.065	0.568
0.850	0.449	1.020	0.596
0.900	0.423	0.976	0.621
0.950	0.398	0.933	0.645
1.000	0.374	0.889	0.670
1.050	0.349	0.846	0.689
1.100	0.325	0.801	0.710
1.150	0.300	0.756	0.726
1.200	0.276	0.710	0.742
1.250	0.251	0.662	0.754
1.300	0.226	0.612	0.764
1.350	0.200	0.559	0.769
1.400	0.173	0.504	0.765
1.450	0.145	0.445	0.752
1.500	0.116	0.382	0.725
1.550	0.086	0.316	0.671
1.600	0.054	0.244	0.564
1.650	0.020	0.167	0.314

REFERENCES

1. "ANSYS ICEM CFD 12.0 User Manual," ANSYS, Inc., April 2009.
2. "Fluent 6.3 User's Guide," Fluent, Inc., September 2006.
3. Neely, Stephen K., "A User Guide to NCBLADE 3.18," November 2005.
4. Rhee, Shin Hyung and Joshi, Shitalkumar, "Computational Validation for Flow around a Marine Propeller Using Unstructured Mesh Based Navier-Stokes Solver," JSME International Journal, 2005.

(THIS PAGE INTENTIONALLY LEFT BLANK)

INITIAL DISTRIBUTION

EXTERNAL DISTRIBUTION

ORG.	NAME (Copies)
NAVSEA	
05D1	Webster
05P16	Crockett, Schumann
ONR	
331	Kim, Joslin
333	Purtell
DTIC	(1)

CENTER DISTRIBUTION

CODE	NAME (Copies)
5030	Jessup
5030	Reed
5060	Walden
5080	Brown
5500	Hughes
5500	Belknap
5700	Miller
5800	Dai
5800	Schroeder
5800	Black
5800	Brown
5800	Fu
5800	Hurwitz
5800	File (2)
3452	Library